On the dependence of simulated convection on domain size

A. M. Jenney[1], **Z. Hu**[2]

[1]College of Earth, Ocean, and Atmospheric Sciences, Oregon State University
[2]Department of Earth and Planetary Sciences, Harvard University

Key Points:

- Deep convection is suppressed in domains with few grid columns due to strong subsidence warming and entrainment into small updrafts
- This effect can be reduced by increasing grid spacing
- Small domains are more humid than large domains regardless of grid spacing because of enhanced convective mixing

Corresponding author: Zeyuan Hu, zeyuan_hu@fas.harvard.edu

Corresponding author: Andrea Jenney, andrea.jenney@oregonstate.edu

Abstract

We present a heuristic model to quantitatively explain the suppression of deep convection in convection-resolving models (CRMs) with small domains. We distinguish between "computational" smallness (few grid columns) and "physical" smallness (representing a small geographic area). Domains that are computationally small require greater instability to sustain convection because they force a large convective fraction, driving strong compensating subsidence warming. Consequently, detrainment occurs lower for undiluted convection. Both computationally and physically small domains limit the physical updraft width, increasing entrainment dilution. This enhancement of entrainment strengthens the sensitivity to domain size beyond that for undiluted deep convection. Coarsening grid spacing to expand the physical domain and physical updraft width can reduce domain size sensitivity. Simulations using the System for Atmospheric Modeling (SAM) confirm the heuristic model results. We also present simulation results for two shallow convection cases, which are less sensitive to domain size, but also exhibit sensitivities.

Plain Language Summary

We present a simple mathematical model that helps explain why cloudy upward air movement (convection) is suppressed in "small" computer simulations used for studying weather. We look at two types of "smallness": one is about the computer's limitations (fewer grid columns), and the other is about how big the area that is being represented would be on a map (physical size). When the computer model has fewer columns, more energy is needed for upward air movement because the compressive warming of sinking air around clouds is stronger. This affects where air stops moving upward (detrainment).

Both types of smallness make the upward air column narrower in a physical sense, causing more outside air to mix in (entrainment). Because cloudy air is typically warmer and more humid than the air around it, this mixing reduces the temperature of the cloudy air and weakens the upward air movement. We found that increasing the number of columns or making the columns wider can help reduce these effects. We tested this in simulations and our results support our simple mathematical model.

1 Introduction

Convection-resolving models (CRMs) are popular tools used to simulate large-scale turbulent motions associated with clouds and convection. In stand-alone simulations, CRMs are oftentimes run with domains as small as 100 km to inhibit the spontaneous clustering of the convective region in a phenomenon known as convective self aggregation (e.g., Wing et al., 2018, 2020), which occurs preferentially in larger domains (Muller & Held, 2012; Yanase et al., 2020). In addition, small CRM domains are often used in general circulation models (GCMs) employing superparameterization (SP), also known as multiscale modeling framework (MMF), in which the convective parameterization is replaced with many embedded CRMs. Recent SP/MMF simulations use CRMs with as few as 64 columns to reduce computational cost (e.g., Hannah et al., 2020, 2022; Lin et al., 2022).

Many studies exploring the sensitivity of standalone CRM simulations to domain size focus on convective self aggregation (Muller & Held, 2012; Patrizio & Randall, 2019; Yanase et al., 2020). These studies have shown that convective self-aggregation tends to occur at domain sizes larger than 200 km. In CRM simulations forced with observations M. F. Khairoutdinov and Randall (2001) find that the precipitable water increased and rainfall fraction decreased with increasing domain size. However, these simulations

varied in dimensionality, horizontal resolution, and vertical resolution, so inferring the isolated impacts of varying domain size is not possible.

Sensitivity to CRM domain size has also been studied in modern SP setups. Liu et al. (2023) compare 2-D simulations of the Energy Exascale Earth System Model-MMF (E3SM-MMF) with 32 total columns to 3-D simulations with 32 grid columns in each horizontal dimension (1024 total columns) and find large differences in mean precipitation and its statistics over some tropical regions. Whether the differences were driven entirely by differences in domain size in the CRMs or by their dimensionality is unclear. Peng et al. (2022) find differences in cloud fractions up to 0.4 and absorbed shortwave radiation up to 60 W m^{-2} in some regions when comparing E3SM-MMF simulations with 32 vs. 64 CRM columns. E3SM-MMF with 2D CRMs with high horizontal resolution (200 m) but small domains (12.8 km) appeared to under-resolve larger eddies important for marine boundary layer clouds (Peng et al., 2023). As in other studies, the different horizontal resolutions associated with different CRM domain sizes of Peng et al. (2022) and Peng et al. (2023) makes disentangling the effects of domain size from horizontal resolution a challenge.

Few studies have explicitly studied the isolated impact of CRM domain size independent of horizontal resolution on convective behavior and the mean atmospheric state for the small domain sizes used in SP models. Pritchard et al. (2014) found that decreasing the CRM domain size from 32 to 8 columns (while keeping horizontal resolution constant) led to an increase in the climate sensitivity of an SP GCM, primarily due to changes in low-level cloudiness. They propose a convective "throttling" hypothesis grounded in buoyancy, in which small CRM domains limit the frequency that deep convection can occur because of strong warming by compensating subsidence occurring over a fractionally smaller area than is possible in a large CRM domain. This occurs because the minimum updraft size is limited by the fraction of the domain occupied by a single grid column, which increases as the number of grid columns decreases. As a result of convective throttling, the lower troposphere remains less ventilated in small CRM domains, resulting in increased lower tropospheric humidity, denser liquid clouds, and a cooler upper troposphere. Despite these differences, the mean tropical radiative cooling rate is insensitive to domain size, which implies a broader distribution of simulated deep convection at the smallest CRM scales due to infrequent yet intense deep convection needed to balance the radiative cooling. These ideas can be traced back to Bjerknes (1938), who provided a similar argument to explain the observed smallness of the tropical updraft fraction.

Despite these advances, a *quantitative* understanding of the mechanisms of the relationship between domain size and mean atmospheric properties remains limited. For example, the domain size at which convergence occurs and how domain size sensitivities interact with horizontal resolution sensitivities (e.g., Jeevanjee & Zhou, 2022) both remain unclear. Motivated by the fact that small domain CRM simulations continue to be run both as standalone simulations and in SP GCMs, this study aims to quantitatively explore the mechanisms proposed in Pritchard et al. (2014) using CRM experiments (i.e., without the host GCM) with relatively "small" domain sizes (i.e., domain sizes smaller than required for convective self-aggregation).

2 Methods

2.1 Experimental Setup

We use the System for Atmosphere Modeling (SAM; Khairoutdinov and Randall 2003), version 6.10.6, configured as a cloud-resolving model. A simple Smagorinsky-type scheme (M. F. Khairoutdinov & Randall, 2003) computes sub-grid scale momentum and scalar tendencies. We run both deep and shallow convective cases.

All deep convective simulations use 60 vertical levels with a model top located near 26km and a rigid-lid top boundary condition. The vertical grid spacing linearly increases from 75m near the surface up to 2.5km, above which it is held constant at 500m. A sponge layer is located above 18km. The radiation scheme is the Rapid and Accurate Radiative Transfer Model for General Circulation Models (RRTMG) (Iacono et al. 2008). We use a constant solar insolation (no diurnal cycle) with fixed solar constant of 683.5 W m-2 and zenith angle of 50.5°. Domain-averaged horizontal wind is nudged to zero at each vertical level with a nudging time scale of 1 hr. Sea surface temperature is fixed uniformly at 303K. Deep convective simulations are initialized from predefined initial temperature and moisture profiles and spun up for 100 days. White noise temperature perturbations on the order of 0.01K are applied to the lowest 5 model layers to initialize convection. Unless otherwise noted, a 20-day period after spin-up is used to compute equilibrium statistics. Domain-mean statistics are sampled every 2 min and then averaged to estimate hourly domain-mean statistics. Instantaneous 3-D fields are saved every 30 minutes.

We present results from 3-D deep convective simulations with 1 km horizontal resolution and 8, 16, 32, 64, 128, 256 grid cells in each horizontal direction ("nx"). To explore interactions between domain size and horizontal resolution sensitivity, we further ran 3 additional sets of simulations with 4km, 250m, and 62.5m resolution. For completeness, we also ran two-dimensional simulations with 16 and 128 columns, which we omit results from because of their close similarity to the 3-D runs.

For shallow convective simulations, We used large scale forcings, boundary conditions, and initial profiles from two field studies: the Barbados Oceanographic and Meteorological EXperiment (BOMEX) (Holland & Rasmusson, 1973) as in Siebesma et al. (2003) to simulate shallow cumulus ("trade" cumulus) and the first research flight of the second Dynamics and Chemistry of Marine Stratocumulus (DYCOMS-RF01) (Stevens et al., 2005) to simulate marine stratocumulus. For these shallow convection simulations, we used a fixed horizontal resolution of 125 m and a fixed vertical resolution of 25 m with 128 vertical levels. The DYCOMS-RF01 simulations are initialized with the same white noise temperature perturbation method as the deep convective simulations. The BOMEX simulations were initialized with white noise temperature perturbations on the order of 0.1 K and water vapor perturbations on the order of 0.025 g kg^{-1} applied to the lowest 1.6 km. Shallow convection simulations were run for 6 hours with a time step of 2 seconds. Unlike the deep convective simulations, here we turned off precipitation. We do not include radiation in the BOMEX simulation, and use a simple interactive longwave radiation calculation as in Stevens et al. (2005) for DYCOMS-RF01. We present results with 8, 16, 32, 64, 128 grid cells in each horizontal direction. Domain-mean statistics are sampled every 20 seconds and then averaged to estimate minute-mean domain-mean statistics.

We ran ensembles of the shallow convective cases to enhance the signal to noise ratio. These ensembles were initialized using different random numbers for the initial white noise perturbation. Most simulations have 64 ensemble members. However, for specific cases, we adjusted the number of members: we present 1024 members for the nx=8 BOMEX case, and 256 members for the nx=16 BOMEX and the nx=16 DYCOMS-RF01 cases.

2.2 Methods for diagnosing entrainment and detrainment rate

In later sections, we will present some results relating to diagnosed fractional entrianment and detrainment rate. Here we document how they are calculated. We first estimate the entrainment and detrainment rate through a simple entraining-detraining bulk-plume model:

$$\frac{\partial \phi_u}{\partial z} = -\epsilon(\phi_u - \phi_n) + S_u \tag{1}$$

$$\frac{1}{M}\frac{\partial M}{\partial z} = \epsilon - \delta \tag{2}$$

where ϕ is a relatively conserved variable, subscripts "u" and "n" denote averages across convective updraft grid cells and non-updraft grid cells, S_u is the net source of ϕ within updraft, ϵ and δ represent the fractional entrainment rate and detrainment rates, and M represents the convective updraft mass flux. Here, we define ϕ_u as the water vapor plus cloud water mixing ratio. S_u is evaporation of precipitation minus cloud-to-precipitation conversion averaged across updraft grid cells, and is zero for our shallow convection simulations where we turned off precipitation. Convective updraft grid cells are those with cloud mixing ratios greater than 10^{-5} kg kg^{-1} and upward vertical velocities greater than 1 m s^{-1}. Non-updraft grid cells are defined as those with cloud water mixing ratios smaller than 10^{-5} kg kg^{-1}. Horizontally averaged ϕ_u, ϕ_n, S_u, and M were saved as part of our domain-mean statistics outputs.

In addition to the above single plume model, we also used a spectrum plume method to diagnose entrainment rate distribution (Kuang & Bretherton, 2006). Unlike the single plume model which assumes all the updrafts have the same entrainment rate profile, the spectrum plume model allows updrafts to have a spectrum of entrainment rates. Here we briefly describe the procedure of calculating entrainment rate distribution used in (Kuang & Bretherton, 2006). First we need to calculate the convective updraft mass flux distribution in the space of frozen moist static energy (FMSE) and height. FMSE is defined as $c_pT+gz+L_vq-L_fq_i$. Then we can specify a set of fractional entrainment rate values, and calculating the FMSE profile of an entraining plume using the mean FMSE in the updraft at the cloud base for each fractional entrainment rate. Then, at each level, we can count how many mass flux falls into each entrainment rate interval according to their FMSE. Essentially we get mass flux distribution in the space of entrainment rate and height.

3 Domain "smallness" and its impacts

Domain size has a clear impact on mean state quantities of limited-domain CRM simulations. For deep convective simulations, Figure 1a-c shows mean profiles of convective mass flux, cloud fraction, and relative humidity, each of which decrease throughout the troposphere with increasing domain size. Larger domains are also colder below 10 km, and warmer above (Figure 1d).

A CRM domain may be small in two ways: it may be computationally small by having few grid columns, and it also may be physically small by covering a small physical area. Increasing the horizontal grid spacing increases the physical domain size of a computationally fixed domain size (i.e., fixed number of grid columns). In the discussion that follows, we will present a heuristic argument to explain how computational smallness leads to convective throttling and how this may be partially compensated by increasing the physical domain size.

The net circulation over a limited domain is the sum of the convective and environmental mass fluxes,

$$\overline{w} = w_c\sigma_c + w_e\sigma_e, \tag{3}$$

where w is vertical velocity, σ is the fractional area of convection (subscript c) and environment (subscript e), and the over bar indicates a domain mean quantity. In writing (3), we have ignored any horizontal variation in density. In both SP-CESM and E3SM-MMF, $\overline{w} = 0$ throughout the CRM domain. We thus omit $\overline{w}$ from subsequent equations.

If environmental air is sinking ($w_e < 0$), it warms due to adiabatic compression at the rate given by $w_e(\Gamma_e - \Gamma_d)$, where $\Gamma = -\partial T/\partial z$ is the lapse rate and Γ_d is the dry adiabatic lapse rate. Using Equation (3) and the fact that the fractional areas of con-

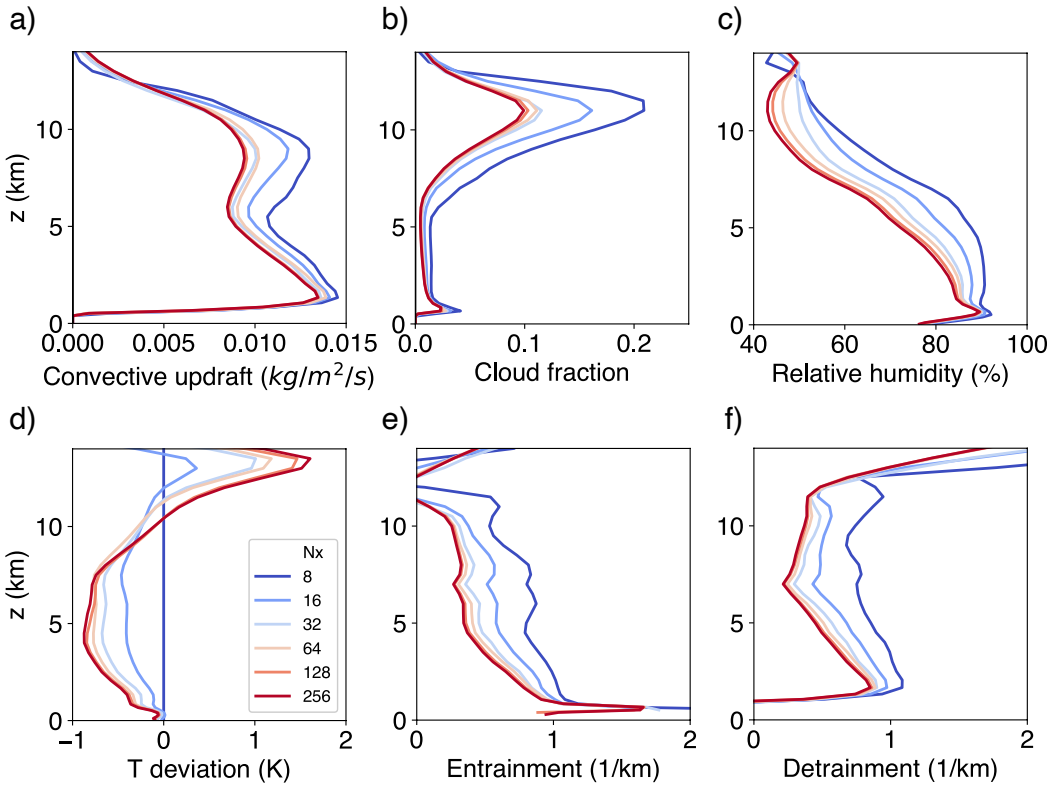

Figure 1. Dependence of atmospheric profiles on domain size for deep convective simulations: (a) updraft mass flux, (b) cloud fraction, (c) relative humidity, (d) temperature deviation from nx=8, (e) fractional entrainment rate and (f) fractional detrainment rate. Entrainment and detrainment are diagnosed using the bulk plume model described in Section 2.2.

vection and of the environment must sum to one, we can write subsidence warming in the descent region as

$$\frac{dT_e}{dt} = -\frac{w_c \sigma_c}{1-\sigma_c}(\Gamma_e - \Gamma_d). \tag{4}$$

The rate that temperature changes in the ascent region during undilute moist convection is

$$\frac{dT_c}{dt} = w_c(\Gamma_c - \Gamma_m), \tag{5}$$

where Γ_m is the saturated adiabatic lapse rate. To sustain a buoyancy-driven convective overturning circulation, positive buoyancy of the convective region is required. This means that the convective region must maintain a positive virtual temperature difference from the surrounding, descending environment. We can approximate this condition as

$$\frac{dT_c}{dt} > \frac{dT_e}{dt}, \tag{6}$$

which we can re-write in terms of the ascent area using Eqs. (4) and (5) as,

$$\sigma_c < \frac{\Gamma_c - \Gamma_m}{\Gamma_d - \Gamma_m + \Gamma_c - \Gamma_e}. \tag{7}$$

Equation (7) describes a limit on the maximum possible fractional convective area in a limited-domain CRM with no mean circulation by the lapse rates of the convective and non-convective region. The largest σ_c that can exist during ongoing convection increases with the instability of the convective region (Γ_c). Conversely, convective area is limited when instability is small. This is a consequence of condition (6). Because subsidence warming is stronger for faster sinking motion, small ascent areas ensure that subsidence warming is weak by being spread over a large area (Bjerknes, 1938). Second, in addition to the instability of the convective region, Equation (7) also shows that horizontal temperature gradients exert a limit on σ_c. When $\Gamma_c - \Gamma_e$ is large, environmental air is more likely to be warmer than convective region air. Thus, convective area must be small for large $\Gamma_c - \Gamma_e$ to keep w_e small and maintain positive convective region buoyancy. In CRM domains using superparameterized models, this effect may be second-order due to the relative smallness of CRM domains and the resulting closeness of Γ_c and Γ_e. For $\Gamma_c \approx \Gamma_e = \overline{\Gamma}$, Equation (7) simplfies to

$$\sigma_c < \frac{\overline{\Gamma} - \Gamma_m}{\Gamma_d - \Gamma_m}. \tag{8}$$

3.1 Small computational domains require more instability to sustain convection

We thus arrive at the first way that small computational CRM domains "throttle" convection. Computational domain size limits the minimum value that σ_c can assume: The smallest possible value of σ_c in a CRM domain is $1/N$ where N is the number of grid columns. This number decreases as the computational domain size and the number of grid columns increases.

For $\Gamma_c \approx \Gamma_e$ (a close approximation in a small domain), the threshold instability (Γ^*) at which a sustained convectly-driven overturning circulation is supported given a minimum possible σ_c (σ_c^*) can be inferred from Equation (8) as:

$$\Gamma^* > \sigma_c^*(\Gamma_d - \Gamma_m) + \Gamma_m \tag{9}$$

Equation (9) shows that as the computational domain size increases and σ_c^* decreases, Γ^* also decreases. As σ_c^* approaches zero, Γ^* approaches Γ_m. Figure 2 shows Γ^* computed from Equation (9) for domains with computational sizes ranging from 2 columns to 512 columns. For undilute convection (solid lines), this critical instability converges for domains larger than about 32 columns (a common number for SP simulations).

Buoyant convection doesn't occur without entrainment. Equation (5) can be modified for entraining convection as

$$\frac{dT_c}{dt} = w_c(\Gamma_c - \Gamma_m - \epsilon\beta) \tag{10}$$

where ϵ is the fractional entrainment rate and β is a dilution factor that depends on the difference in temperature and humidity between the updraft air and the entrained air, which we will crudely approximate as

$$\beta = T_c - T_e + \frac{L_v}{c_p}(q_s - q_e). \tag{11}$$

In Equation (11), L_v is the latent heat of vaporization, c_p is the specific heat capacity of dry air, and q is the water vapor mixing ratio. In writing (11), we have assumed that the entrained air has the temperature and humidity of the environment and that the convective region is saturated (q_s). We have also neglected differences in latent heating due to ice processes.

When the effects of entrainment are considered in the dependence of $\Gamma*$ on domain size, convergence at large domain sizes diminishes. We illustrate this with an example in Figure 2, which shows $\Gamma*$ profiles computed using a modification of Equation (9) that includes entrainment with (10) and (11). We neglect temperature differences between the convective and non-convective region ($T_c - T_e = 0$). We apply a 1% decrease in the relative humidity for successive domain sizes (as in Figure 1c), and entrainment rates which decrease by 5% as the number of columns is doubled (as in Figure 1e; see Section 3.2). Figure 2 shows that incorporating the impact of entrainment on $\Gamma*$ reduces large domain size convergence. This is a consequence of the sensitivity of the entrainment rate to domain size (which we discuss in the next section), despite a contribution in the opposite direction by the spread in relative humidity with domain size.

In summary, one way small computational domains "throttle" convection is by requiring more instability to sustain convection due to large σ_c. As we will show in the next section, entrainment rates also decrease as domain size decreases. As a result, while there is convergent behavior in Γ^* for domains larger than 32 columns for undilute convection, differences in entrainment reduce this convergence, and differences in Γ^* with domain size exist even for computationally large domains.

3.2 Small domains limit updraft width and enhance convective mixing

The critical instability in Equation (9) is the threshold lapse rate for *one grid column* to buoyantly convect without violating condition (6). For a given value of $\Gamma > \Gamma^*$, the number of grid columns available for convection increases with the computational domain size. This implies, for a fixed grid size, that increasing the total number of columns also allows updrafts to be *physically* wider. Convective entrainment rates are larger for physically small updrafts (Morrison, 2017; Morrison et al., 2020). Thus, the second way that CRM domain size "throttles" convection is by limiting updraft width and reducing updraft buoyancy by enhancing dilution by entrainment.

Our simulations are consistent with this behavior. Figure 1e shows that the mean fractional entrainment rate decreases with increasing computational domain size (for a fixed grid spacing). This occurs because updrafts are forced to be physically small in small domains. Figure 3 shows distributions of entrainment rate and updraft width at 8 km

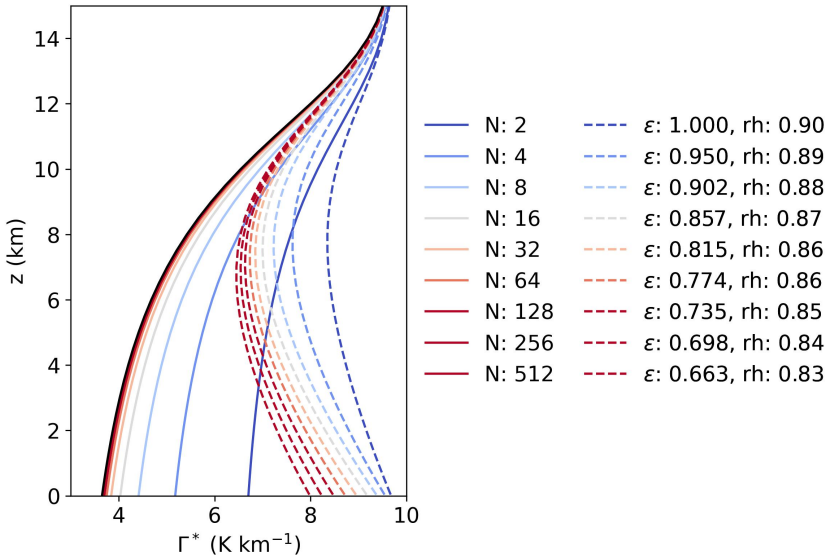

Figure 2. The critical lapse rate, Γ^*, needed to sustain a convective overturning circulation from Equation (9) for domains of different computational sizes. Here, "N" refers to the total number of grid columns. Solid lines show $\Gamma*$ for undilute convection. Dashed lines show $\Gamma*$ when idealized entrainment dilution is considered. Entrainment rates and relative humidities, which vary with the number of columns, (km $^{-1}$) are shown in the legend. Black line is the moist adiabatic lapse rate for a surface temperature of 300 K.

for square domains with 16, 64, and 256 columns in each horizontal dimension. As expected, updrafts are narrower in the small domain and entertainment rates are larger. The other two domain sizes are more similar, yet exhibit differences in line with our expectations: the largest domain has slightly larger updrafts and slightly weaker entrainment rates.

For a small domain (such that $\sigma_c \approx \sigma_c^*$) at a computationally fixed size, increasing the grid spacing will make updrafts physically wider. Thus, we expect that they should also entrain less (Morrison, 2017; Morrison et al., 2020). Additional simulations with varying horizontal resolution corroborate this expectation. Figure 4m-p shows entrainment rates for simulations with a range of computational domain sizes as grid spacing is decreased from 4 km (left) to 62.5 m (right). As the grid spacing decreases and updrafts become smaller, the distribution of entrainment rates shifts towards larger values. Differences in the entrainment rate between resolutions are largest for the smallest domain.

In summary, computationally small domains increase convective entrainment rates because they limit updraft width. This impact can be reduced either by increasing the physical or computation domain size.

3.3 Convection in small domains detrains lower

Computationally small domains limit the minimum possible value that σ_c can assume. As a result of σ_c that is forced to be large, updrafts are inhibited by too-strong compensating subsidence (Section 3.1). In Section 3.2, we discussed how domain size limits updraft width, and enhances entrainment. It can be intuited that detrainment should also occur lower in small domains as a result of these combined effects. This is confirmed in our simulations. Figures 1f and 4q-t show that detrainment in simulated convection

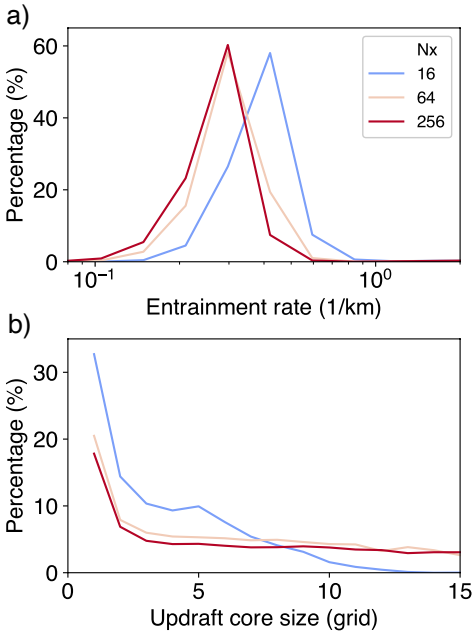

Figure 3. Probability distributions of (a) entrainment rate and (b) updraft width at 8 km. The entrainment rate distribution is diagnosed using the spectrum plume model described in Section 2.2. The core size distribution is calculated as the mass-flux-weighted number of updraft grid cells in each contiguous updraft core. A single core is determined as adjacent grid cells with upward velocity greater than 1 m s^{-1} and cloud mixing ratio greater than 10^{-5} kg kg^{-1}.

increases as computational domain sizes decreases. This is expected behavior even for undilute convection.

Entrainment enhances this behavior. Updraft buoyancy reduction due to dilution by entrainment is more likely as domain size decreases and updrafts become smaller. In this way, enhanced entrainment also increases the impact of domain size on detrainment. Figure 4q-t shows that as grid spacing decreases (and differences in entrainment between computational domain sizes increases), the spread in detrainment rate with domain size also increases, with the smallest domains at this highest resolution detraining the most.

3.4 Domain size impacts on mean state variables and precipitation variability

The mean relative humidity decreases with increasing computational and physical domain size (Figure 1c, Figure 4a-d). This is consistent with the sensitivity of entrainment and detrainment to domain size (see Romps, 2014), both of which increase as domains (and their updrafts) become smaller. Unlike detrainment and entrainment, which display narrowing distributions across computational domain sizes as grid spacing is increased, the distribution of relative humidity does not narrow–it only shifts towards lower values. Jeevanjee and Zhou (2022) discuss the sensitivity of relative humidity to horizontal resolution.

A higher relative humidity in small domains implies that convection is less efficient at heating the atmosphere due to enhanced evaporation. This explains why the convective mass flux is larger for small domains (Figure 1a, Figure 4e-h). High cloud fractions are also larger in small domains (Figure 1b). This is likely contributed to by the larger

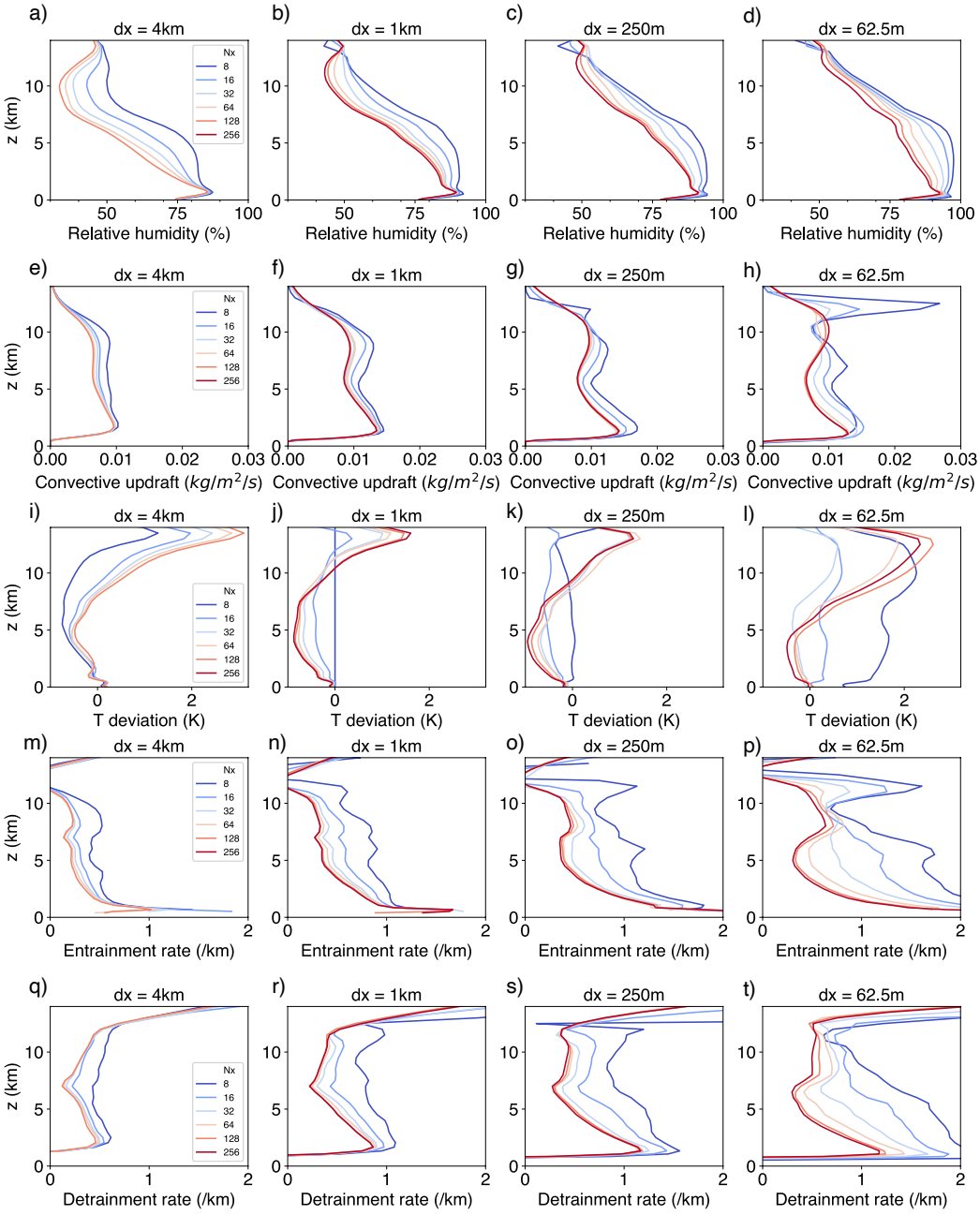

Figure 4. Sensitivity of domain mean profiles to computational domain size across horizontal resolutions of (left column), 1km (center left column), 250 m (center right column), and 62.5 m (right column). The rows from top-to-bottom are: (a-d) relative humidity, (e-h) updraft mass flux, (i-l) temperature deviation from nx=8, (m-p) fractional entrainment rate, and (q-t) fractional detrainment rate. Entrainment and detrainment are diagnosed using the bulk plume model described in Section 2.2.

convective mass flux below the anvil level, which provides a larger anvil cloud source rate, as well as the higher relative humidity, which slows anvil cloud evaporation (Beydoun et al., 2021; Seeley et al., 2019). The change of temperature profiles may be viewed as mixture of two effects. On one hand, the stronger entrainment in the smaller domain tends to pull the temperature lapse rate away from moist pseudoadiabat lapse rate, making the temperature colder in smaller domain (Figure 4i). On the other, smaller domain also tends to have larger anvil cloud fraction and cloud radiative heating through the troposphere, which increases the temperature below anvil cloud in smaller domains (Figure 4j-l).

Figure 5 shows time series of precipitation, convective available potential energy (CAPE), and w_e. In addition to being higher, on average, the temporal variability of instability is also larger for small domains. The higher mean value of CAPE is a consequence of Equation (9): for small domains, the lapse rate needs to be larger (more unstable) to maintain a convective overturning circulation. In small domains, this manifests as periods of quiescence, when convection is suppressed, interspersed with periods of intense convection that occur when radiative cooling sufficiently steepens the lapse rate. In comparison, domain mean CAPE and precipitation are more consistent in time for large domains. This occurs, in part, because σ_c can be small in large domains, and consequently less instability is needed to maintain a convective circulation. The decreasing temporal variance with increasing computational domain size may also be contributed to by the increasing sample size.

4 Shallow convective cases

The heuristic argument of Section 3 hinges on the buoyancy condition that the rate of change of temperature in the convective region be larger than that of the subsiding non-convective region (Equation 6), and the implicit assumption that this condition must be satisfied in order for motion in the convective region to be ascending. While this is reasonable for deep convection, this may not capture the behavior of shallow convection as closely. For example, the boundary layer eddies that help maintain marine stratocumulus clouds are largely driven by strong radiative cooling at their tops (reviewed in Wood, 2012). Thus for completeness, we also tested the sensitivity of two shallow convective cases to computational domain size, described in Section 2.1. We used the BOMEX case to simulate trade cumulus, and we used the DYCOMS-RF01 case to simulate stratocumulus.

Figure 6 shows the 6-hour time series of cloud properties in the shallow convective simulations. Temporal variability for the small domains is much larger, likely due to the simulation only capturing the evolution of one or a small number of convective updrafts at a time. To enhance the signal-to-noise ratio of our results, we ran ensembles described in Section 2.1. The solid lines in Figure 6 represent the ensemble mean, while the shading represents the ensemble spread between the 25th to 75th quantiles. For both the BOMEX and DYCOMS-RF01 cases, the time evolution of cloud fraction and cloud water path converges for domains with at least 32×32 columns.

For the BOMEX case (Figure 6 left column), the smallest domain (nx=8) shows significantly reduced cloud water path and slightly elevated cloud fraction compared to larger domains. These differences can also be viewed in the vertical profiles averaged over the last 2 hours (Figure 7). The updraft mass flux in nx=8 has a very similar maximum value around 750 m but is shallower than the larger domains (Figure 7a). The faster decline of the updraft mass flux above the maximum indicates stronger detrainment (Figure 7d). This, taken together with the stronger diagnosed entrainment in nx=8 (Figure 7c) is consistent with our result of stronger mixing for small domains from the deep convective simulations.

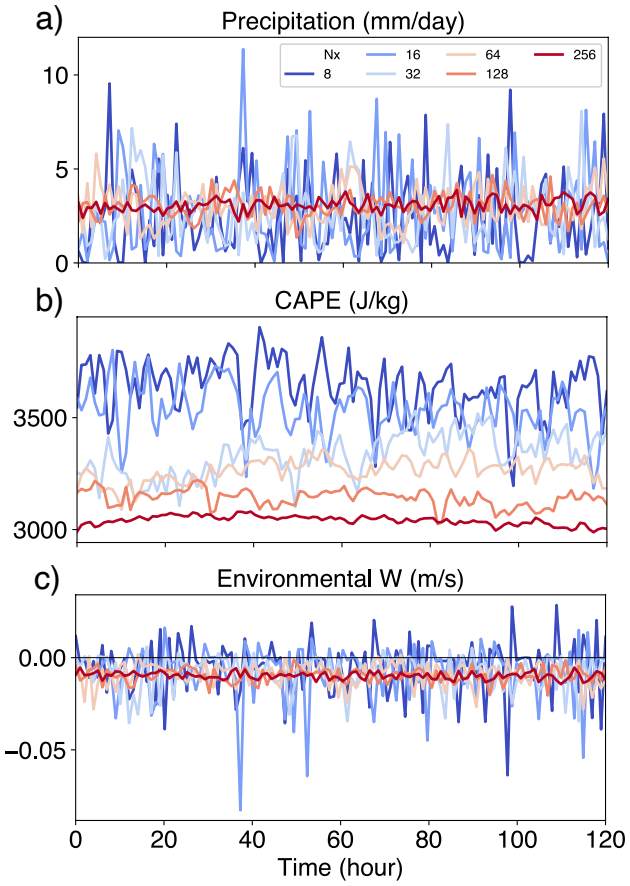

Figure 5. Time series of (a) surface precipitation, (b) convective available potential energy (CAPE), and (c) environmental vertical velocity across 5 days.

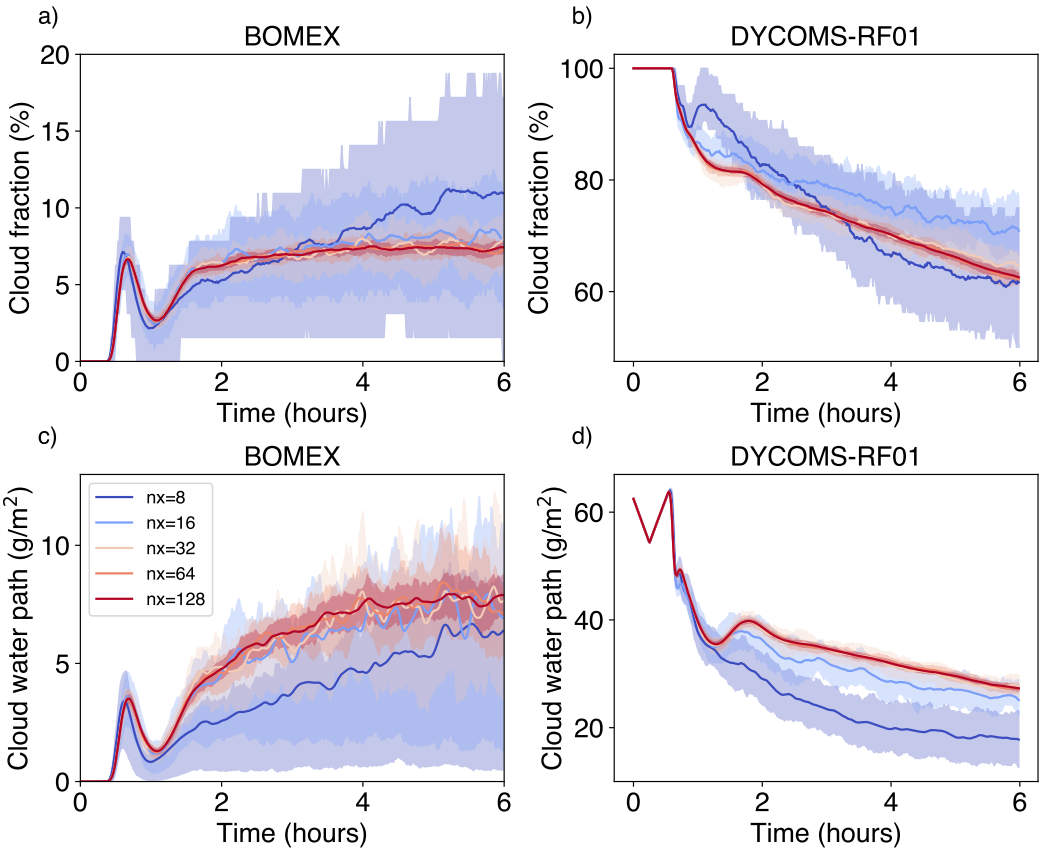

Figure 6. Time series of vertically integrated cloud fraction (top row) and cloud water path (bottom row) for the BOMEX case (left column) and the DYCOMS-RF01 case (right column). Solid lines are the ensemble mean, and the shading represents the 25th to 75th percentile of the ensemble spread. Cloud fraction here is defined as fraction of columns that have a cloud water path larger than 10 g m^{-2}.

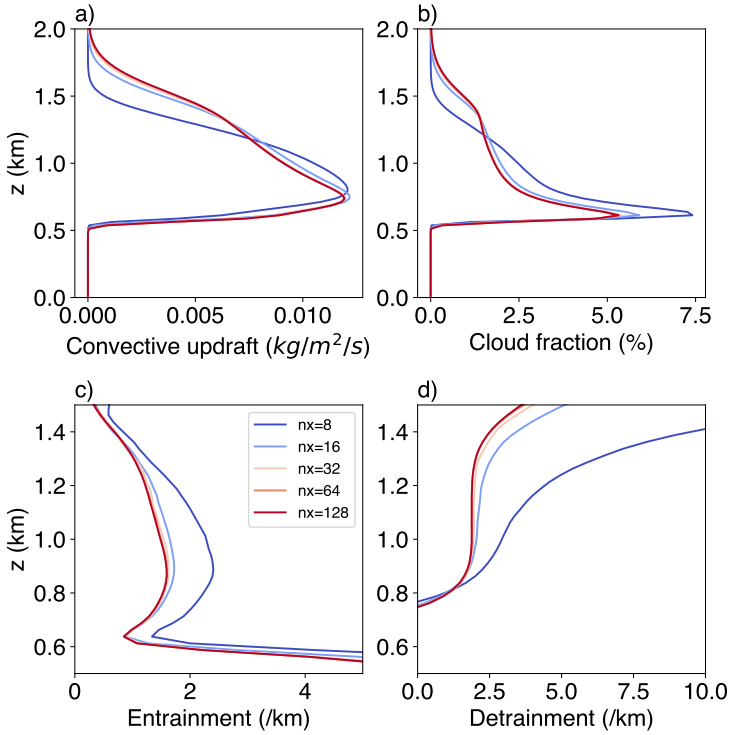

Figure 7. Mean atmosphere profiles over the last 2 hours in the BOMEX simulations: (a) updraft mass flux, (b) cloud fraction, (c) the fractional entrainment rate, and (d) the fractional detrainment rate. Entrainment and detrainment are diagnosed using the bulk plume model described in Section 2.2.

For the DYCOMS-RF01 stratocumulus case (Figure 6 right column), there is a significant reduction in the cloud water path for the two smaller domain sizes. For nx=8 and nx=16, some ensemble members are able to sustain a larger cloud fraction than the larger domains. In nx=8, the stratocumulus cloud decks fully dissipate for some ensemble members (not shown). This may suggest that our smallest domain with 8×8 columns (1km×1km) is too small to sufficiently simulate stratocumulus and may trigger an instability that is sensitive to the initial noise perturbation. We encourage future studies to further explore this instability.

5 Summary

In simulations using convection resolving models (CRMs), small domains are used in both standalone simulations and within GCMs employing superparameterization or a multi-scale modeling framework. A CRM domain can be computationally small by having few grid columns, and it can also be physically small by representing a small physical area.

Convective fractional area must be small in order to maintain positive buoyancy against a subsiding and warming environment. Small convective fractional area ensures that the downward mass flux is spread over a large area and hence, heats the environment slowly. This is the same argument used to explain the observed smallness of the tropical convective ascent area (Bjerknes, 1938). In CRM domains, the smallest possible convective fractional ascent area increases as the number of total grid columns decreases. Consequently, convective fractional ascent area is forced to be large in CRM do-

mains with few grid columns and subsidence warming is strong, which suppresses convection. This argument is presented qualitatively in Pritchard et al. (2014).

Here, we present a heuristic argument to show why convection is "throttled", or suppressed, in small domains. We show that

1. Small computational domains require more instability to sustain convection due to large convective fractional areas.
2. Physical updraft width is limited in both computationally and physically small domains, which increases updraft dilution by entrainment. This impact can be reduced by increasing the grid spacing and by increasing the number of columns.
3. Detrainment occurs lower in the atmosphere for undilute convection in small domains. This is enhanced by the impact of domain size on updraft width and subsequent entrainment dilution.

As a result of "throttled" convection, the domain mean instability increases for small domains, and precipitation becomes more temporally variable, with periods of intense rain followed by relatively quiescent periods. Enhanced entrainment and detrainment in small domains increases the mean relative humidity, convective mass flux, and anvil cloud fraction. These conclusions are supported with CRM simulations of radiative convective equilibrium.

We also present results from shallow convective simulations across a range of domain sizes for a shallow cumulus case and a marine stratocumulus case. In both cases, we see convergence of cloud properties when we increase the domain size. Similar to the deep convection simuluations, the shallow cumulus simulations also show stronger entrainment and detrainment rate in the small domains, leading to shallower updraft mass flux and cloud fraction. For the stratocumulus case, small domain seems to be more unstable for cloud deck to maintain. This may suggest that it is insufficient to capture all the relevant processes for stratocumulus dynamics in a very small domain.

6 Discussion

An important new finding here is the suppression of convection that results from the limitation of updraft width by small domains, and subsequent strong entrainment dilution. This helps explain why simulated mean fields can still differ across larger domains, despite the expectation of convergent behavior beyond 32 columns for undiluted convection. We expect entrainment rates, and subsequent domain size sensitivity, to roughly converge at the domain size where the physical updraft width distribution is insensitive to domain size. In SAM, this occurs for domains with around 128×128 columns. Because this number is smaller for coarse grid spacing, we recommend using low horizontal resolution for small computational domains simulating deep convection to avoid suppression of deep convection. Additionally, the suggested domain sizes exhibiting convergence depend on entrainment and may be model dependent, as entrainment mixing relies, in part, on sub-grid schemes. Therefore, while all CRMs should show sensitivity to domain size, the precise size where convergence occurs could vary by model.

This study has direct implications for superparameterized modeling, which continues to use computationally small domains because of the demanding computational cost. Pritchard et al. (2014) evaluate the climate of SP-GCM simulations with 8, 16, and 32 columns in the embedded CRMs. A key result of their study was a stronger tropical shortwave cloud forcing, which resulted from enhanced low-level liquid cloud and a drier and less cloudy upper troposphere. Also, the simulations with the smallest CRM domain produced more low intensity precipitation and less high intensity precipitation. These results differ from our results here. Our smallest domain simulations exhibit higher humidities throughout the troposphere, higher anvil cloud fractions, and a wider precip-

itation distribution. We hypothesize that these differences can be explained by circulations on the GCM grid that move energy between CRM domains in the SP setup. In an SP-GCM, convection can be continually suppressed in convectively stable regions because the CRM domain is not in energy balance. Conversely, in our simulations, the absence of a large-scale circulation means that convection has to happen somewhere in the domain to balance radiative cooling.

The convective area fraction's tight control by the domain lapse rate is in part a result of domain mass conservation ($\overline{w} = 0$). We can write the condition for convection (6) because it is always true that environmental air is descending if there is convection occuring. Consider however the case where $\overline{w} \neq 0$, for example in an SP-GCM where the CRM directly experiences the large-scale vertical motion of a host grid cell. Assuming condition (6) holds, (7) becomes

$$\sigma_c < \frac{\Gamma_c - \Gamma_m - \frac{\overline{w}}{w_c}}{\Gamma_d - \Gamma_m + \Gamma_c - \Gamma_e}. \tag{12}$$

If $\overline{w} < 0$, condition (6) is still valid. However, convection may be less "throttled" because the descending mean mass flux enables a larger maximum σ_c. That is, for a given computational domain size, convection may be triggered for less unstable profiles than is possible when $\overline{w}$ *must* be zero. For large-scale ascent ($\overline{w} > 0$), environmental air is no longer guaranteed to be sinking and warming, and we can not claim (12) because of the potential for violation of condition (6). Currently, in both E3SM-MMF and SP-CESM, any large-scale vertical motion occurring on the GCM grid is communicated to the embedded CRM via a horizontally uniform forcing on the temperature (and moisture) tendencies (Grabowski, 2001), rather than on the velocity field. This does not impact the limitation of convective fractional ascent by the local lapse rate written in Equation (7). It remains to be seen if convective throttling is reduced in superparameterized simulations without strict enforcement of $\overline{w} = 0$.

Lastly, while quantitative, the argument we use to explain why a small CRM domain "throttles" convection relies on a minimalist depiction of relations between variables during convective motions. For example, radiation, which is not considered in our equations, may help reduce the critical lapse rate (Γ^*) needed to sustain an overturning circulation for a given computational domain size because it heats the convective region relative to the non-convective region and thus helps maintain condition (6). Similarly, we do not consider cooling in the environmental region due to evaporation of detrained condensate, which may further help to reduce Γ^*. It is possible that these processes may have stronger effects than we anticipate. While entrainment is considered in a mostly qualitative sense in our discussion of the limitation of updraft width by domain size, we show in Figure 2 that it can have a large impact on Γ^*. Nonetheless, we believe that the model captures the primary relationships between variables that help explain convective throttling in small domains.

7 Data and Software Availability

Convection resolving model simulations were conducted with the System for Atmospheric Modeling (SAM) version 6.10.6 (M. Khairoutdinov, 2022).

Acknowledgments

This research has been supported by the National Oceanic and Atmospheric Administration Climate & Global Change Postdoctoral Fellowship Program through UCAR CPAESS Grant no. NA18NWS4620043B. This work used Bridges-2 at Pittsburgh Supercomputing Center through allocation EES230034 from the Advanced Cyberinfrastructure Coordination Ecosystem: Services & Support (ACCESS, Boerner et al., 2023) program, which is supported by National Science Foundation grants 2138259, 2138286, 2138307, 2137603,

and 2138296. We thank Zhiming Kuang, Kerry Emanuel, Xueying Yu, and Roger Samelson for helpful comments.

References

Beydoun, H., Caldwell, P. M., Hannah, W. M., & Donahue, A. S. (2021, August). Dissecting anvil cloud response to sea surface warming. *Geophys. Res. Lett.*, *48*(15).

Bjerknes, J. (1938). Saturated-adiabatic ascent of air through dry-adiabatically descending environment. *Quart. J. Roy. Meteor. Soc.*, *64*, 325–330.

Boerner, T. J., Deems, S., Furlani, T. R., Knuth, S. L., & Towns, J. (2023, September). ACCESS: Advancing innovation: NSF's advanced cyberinfrastructure coordination ecosystem: Services & support. In *Practice and experience in advanced research computing* (pp. 173–176). New York, NY, USA: Association for Computing Machinery.

Grabowski, W. W. (2001, May). Coupling cloud processes with the Large-Scale dynamics using the Cloud-Resolving convection parameterization (CRCP). *J. Atmos. Sci.*, *58*(9), 978–997.

Hannah, W. M., Jones, C. R., Hillman, B. R., Norman, M. R., Bader, D. C., Taylor, M. A., ... Lee, J. M. (2020, January). Initial results from the superparameterized E3SM. *J. Adv. Model. Earth Syst.*, *12*(1).

Hannah, W. M., Pressel, K., Ovchinnikov, M., & Elsaesser, G. (2022). Checkerboard patterns in E3SMv2 and E3SM-MMFv2. *Geoscientific Model Development*, *15*(15), 6243–6257.

Holland, J. Z., & Rasmusson, E. M. (1973, January). Measurements of the atmospheric mass, energy, and momentum budgets over a 500-kilometer square of tropical ocean. *Mon. Weather Rev.*, *101*(1), 44–55.

Jeevanjee, N., & Zhou, L. (2022, March). On the resolution-dependence of anvil cloud fraction and precipitation efficiency in radiative-convective equilibrium. *J. Adv. Model. Earth Syst.*, *14*(3).

Khairoutdinov, M. (2022). *System for Atmospheric Modeling (version 6.10.6) [Software].* `http://rossby.msrc.sunysb.edu/~marat/SAM/`.

Khairoutdinov, M. F., & Randall, D. A. (2001, September). A cloud resolving model as a cloud parameterization in the NCAR community climate system model: Preliminary results. *Geophys. Res. Lett.*, *28*(18), 3617–3620.

Khairoutdinov, M. F., & Randall, D. A. (2003, February). Cloud resolving modeling of the ARM summer 1997 IOP: Model formulation, results, uncertainties, and sensitivities. *J. Atmos. Sci.*, *60*(4), 607–625.

Kuang, Z., & Bretherton, C. S. (2006). A mass-flux scheme view of a high-resolution simulation of a transition from shallow to deep cumulus convection. *Journal of the Atmospheric Sciences*, *63*(7), 1895–1909.

Lin, G., Jones, C. R., Leung, L. R., Feng, Z., & Ovchinnikov, M. (2022, January). Mesoscale convective systems in a superparameterized E3SM simulation at high resolution. *J. Adv. Model. Earth Syst.*, *14*(1).

Liu, N., Pritchard, M. S., Jenney, A. M., & Hannah, W. M. (2023, April). Understanding precipitation bias sensitivities in E3SM-multi-scale modeling framework from a dilution framework. *J. Adv. Model. Earth Syst.*, *15*(4).

Morrison, H. (2017, March). An analytic description of the structure and evolution of growing deep cumulus updrafts. *J. Atmos. Sci.*, *74*(3), 809–834.

Morrison, H., Peters, J. M., Varble, A. C., Hannah, W. M., & Giangrande, S. E. (2020, October). Thermal chains and entrainment in cumulus updrafts. part i: Theoretical description. *J. Atmos. Sci.*, *77*(11), 3637–3660.

Muller, C. J., & Held, I. M. (2012, August). Detailed investigation of the Self-Aggregation of convection in Cloud-Resolving simulations. *J. Atmos. Sci.*, *69*(8), 2551–2565.

Patrizio, C. R., & Randall, D. A. (2019, July). Sensitivity of convective self-aggregation to domain size. *J. Adv. Model. Earth Syst.*, *11*(7), 1995–2019.

Peng, L., Pritchard, M., Blossey, P. N., Hannah, W. M., Bretherton, C. S., Terai, C. R., & Jenney, A. M. (2023). Improving stratocumulus cloud amounts in a 200-m resolution multi-scale modeling framework through tuning of its interior physics. *ESS Open Archive*.

Peng, L., Pritchard, M., Hannah, W. M., Blossey, P. N., Worley, P. H., & Bretherton, C. S. (2022, May). Load-balancing intense physics calculations to embed regionalized high-resolution cloud resolving models in the E3SM and CESM climate models. *J. Adv. Model. Earth Syst.*, *14*(5).

Pritchard, M. S., Bretherton, C. S., & DeMott, C. A. (2014, September). Restricting 32-128 km horizontal scales hardly affects the MJO in the superparameterized community atmosphere model v.3.0 but the number of cloud-resolving grid columns constrains vertical mixing. *J. Adv. Model. Earth Syst.*, *6*(3), 723–739.

Romps, D. M. (2014, October). An analytical model for tropical relative humidity. *J. Clim.*, *27*(19), 7432–7449.

Seeley, J. T., Jeevanjee, N., Langhans, W., & Romps, D. M. (2019, January). Formation of tropical anvil clouds by slow evaporation. *Geophys. Res. Lett.*, *46*(1), 492–501.

Siebesma, A. P., Bretherton, C. S., Brown, A., Chlond, A., Cuxart, J., Duynkerke, P. G., ... Others (2003). A large eddy simulation intercomparison study of shallow cumulus convection. *J. Atmos. Sci.*, *60*(10), 1201–1219.

Stevens, B., Moeng, C.-H., Ackerman, A. S., Bretherton, C. S., Chlond, A., de Roode, S., ... others (2005). Evaluation of large-eddy simulations via observations of nocturnal marine stratocumulus. *Monthly weather review*, *133*(6), 1443–1462.

Wing, A. A., Reed, K. A., Satoh, M., Stevens, B., Bony, S., & Ohno, T. (2018, March). Radiative–convective equilibrium model intercomparison project. *Geoscientific Model Development*, *11*(2), 793–813.

Wing, A. A., Stauffer, C. L., Becker, T., Reed, K. A., Ahn, M., Arnold, N. P., ... Zhao, M. (2020, July). Clouds and convective Self-Aggregation in a Multi-Model ensemble of Radiative-Convective equilibrium simulations. *J. Adv. Model. Earth Syst.*.

Wood, R. (2012, August). Stratocumulus clouds. *Mon. Weather Rev.*, *140*(8), 2373–2423.

Yanase, T., Nishizawa, S., Miura, H., Takemi, T., & Tomita, H. (2020, August). New critical length for the onset of self-aggregation of moist convection. *Geophys. Res. Lett.*, *47*(16).